

# A Novel MC-DTC Method for Induction Motor Based on Fuzzy-neural Network Space Vector Modulation

Bin-jun Cai<sup>1,2</sup>, Xiao-hong Nian<sup>1</sup>

1. School of Information Science and Engineering, Central South University, Changsha, China

2. Hunan Institute of Engineering, Xiangtan, China

**Abstract**—To improve the low speed performance of the direct torque control(DTC) system. The advantages of DTC method are combined with the advantages of the matrix converter based on space vector modulation technique. The design process of the neural network controller which generating the flux reference voltage vector and fuzzy controller which applying the torque reference voltage vector were represented. This proposed novel method provides a precious input power factor control capability beside the high control performances. Furthermore, Conventional principles of DTC and space vector modulation(SVM) of matrix converter(MC) were described. The combination of the two was given in detail. Finally, the simulation and experiment research were carried out to identify the new method effectiveness. The results of induction motor control at both steady state and transient state are shown to improve the low-speed performance and strong adaptability of novel control strategy.

**Index Terms**—DTC;MC;SVM;Fuzzy-neural network; low-speed performance

## I. INTRODUCTION

Direct torque control (DTC) is a novel high-performance control strategy in the field of AC drives. Since the Direct Torque Control method has been proposed in the middle of 1980's, DTC method becomes one of the high performance control strategies for AC machine to provide a very fast torque and flux control [1],[2]. There are no requirements for coordinate transformation, no requirements for PWM generation and current regulators. It is widely known to produce a quick and fast response in AC drives by selecting the proper voltage space vector according to the switching status of inverter which is determined by the error signal of reference flux linkage and torque with their estimated values and the position of the estimated stator flux. Some research is being done to adapt DTC to new converters and also to reduce the torque ripple, which is one of its main drawbacks. DTC is the direct control of torque and flux of a drive by the selection, through a look-up table, of the inverter voltage space vectors. The main advantage of DTC is its structure, no coordinate transformations and no PWM generation are needed. However, torque and flux modulus values and the sector of the flux are needed. Not only it is a very simple and robust signal processing scheme but also a very quick and precise

torque control response is achieved. Compared with complex coordinate transformation in vector control, DTC can be realized easily in digital with simple structure. While problems are existed as follows as well. Firstly, the switching frequency of voltage source inverter is Non-Fixing. Non-Fixing switching frequency cause switching capability of the inverter not to be used fully[3], [4]. Secondly, there is sharp increase or decrease of torque because only one voltage vector works in a sampling period and the options of vector is limited [5]. Fuzzy logic control has manifested its robustness, and has been extensively researched and used as one of the intelligent control methods in control field [6],[7],[8]. To further improve the performance of torque control and to enhance the system robustness, a novel SVM-DTC strategy of induction motors has been proposed. The new SVM-DTC strategy uses fuzzy-neural network controller to substitute the original PI controller.

In this paper, the DTC-SVM is proposed which allows the generation of the voltage vectors required to implement the DTC of induction motor, furthermore, the input power factor is continuously controlled to be in phase with the input line-to-neutral voltage vector based on the direct SVM technique. The appropriate switching configurations of the matrix converter for each constant time are presented in an opportune switching table[9],[10],[11]. To further improve the performance of torque control The table is only entered by the imaginary voltage vector, which is generated from the conventional DTC method for voltage source inverter, and the position of input voltage vector which can be measured exactly, respectively. Simulation and experiment at the high-speed and low-speed are carried out to prove the good performances of the novel method.

## II. CONVENTIONAL DIRECT TORQUE CONTROL

### A. Mathematical mode of induction machine

Direct torque control system applies mathematical analysis about space vector. The mathematical mode of induction machine is shown in Fig. 1.

$$\psi_{as} = \int (v_{as} - R_s i_{as}) dt \quad (1)$$

$$\psi_{\beta s} = \int (v_{\beta s} - R_s i_{\beta s}) dt \quad (2)$$

According to Fig. 1 flux-linkage equations of induction machines in the stator stationary reference frame as follows.

Where  $\psi_{\alpha s}$  and  $\psi_{\beta s}$  are the  $\alpha$ -axis and  $\beta$ -axis component of  $\vec{\psi}_s$  respectively;  $v_{\alpha s}$  and  $v_{\beta s}$  are the  $\alpha$ -axis and  $\beta$ -axis component of  $\vec{v}_s$  respectively;  $i_{\alpha s}$  and  $i_{\beta s}$  are the  $\alpha$ -axis and  $\beta$ -axis component of  $\vec{i}_s$  respectively.

The electromagnetic torque can be expressed using the following equation.

$$T_e = \frac{3}{2} n_p (\vec{\psi}_s \times \vec{i}_s) = \frac{3}{2} n_p (\psi_{\alpha s} i_{\beta s} - \psi_{\beta s} i_{\alpha s}) \quad (3)$$

Where  $T_e$  is electromagnetic torque and  $n_p$  is the number of rotor pole pairs.

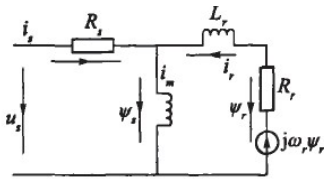


Figure 1. The mathematical mode of induction motor

**B. Principle of direct torque control**

The basic principle in conventional DTC for induction motors is to directly select stator voltage vectors by means of a hysteresis stator flux and torque control. As it is shown in Fig. 2.

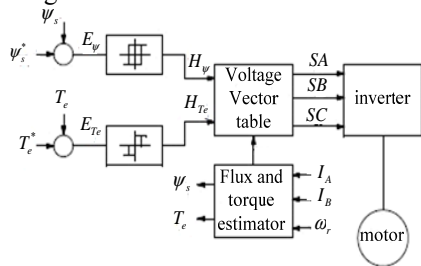


Figure 2. The diagram block of basic DTC

From Fig. 2 can obtain stator flux  $\psi_s^*$  and torque  $T_e^*$  references are compared with the corresponding estimated values. Both stator flux and torque errors,  $E_{\psi}$  and  $E_{T_e}$ , are processed by means of a hysteresis band comparators. In particular, stator flux is controlled by a two-level hysteresis comparator, whereas the torque is controlled by a three-level comparator. On the basis of the hysteresis comparators and stator flux sector a proper VSI voltage vector is selected by means of the switching table given in Tab. I

TABLE I. BASIC DTC SWITCHING TABLE

Sector of Flux →	1	2	3	4	5	6
$c_T = 0$	$c_T = -1$	$V_{2-VSI}$	$V_{3-VSI}$	$V_{4-VSI}$	$V_{5-VSI}$	$V_{6-VSI}$
	$c_T = 0$	$V_{7-VSI}$	$V_{0-VSI}$	$V_{7-VSI}$	$V_{0-VSI}$	$V_{0-VSI}$
	$c_T = 1$	$V_{6-VSI}$	$V_{1-VSI}$	$V_{2-VSI}$	$V_{3-VSI}$	$V_{4-VSI}$
$c_T = +1$	$c_T = -1$	$V_{3-VSI}$	$V_{4-VSI}$	$V_{5-VSI}$	$V_{6-VSI}$	$V_{1-VSI}$
	$c_T = 0$	$V_{0-VSI}$	$V_{7-VSI}$	$V_{0-VSI}$	$V_{7-VSI}$	$V_{0-VSI}$
	$c_T = 1$	$V_{5-VSI}$	$V_{6-VSI}$	$V_{1-VSI}$	$V_{2-VSI}$	$V_{3-VSI}$

**III. THE FUZZY-NEURAL NETWORK SVM-DTC SCHEME**

**A. Fuzzy-neural network SVM-DTC scheme**

The voltage vector can compensate the flux linkage error and torque error is named reference voltage vector. The core issue of SVM-DTC algorithm is how to obtain the reference voltage vector. Fig. 3 is principle block diagram of improved SVM-DTC.

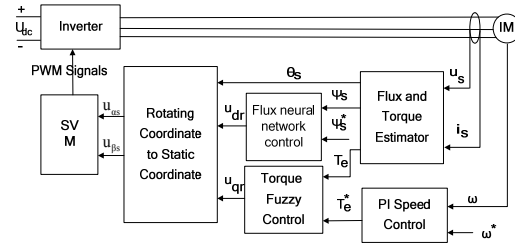


Figure 3. Fuzzy-neural network SVM-DTC system block-diagram

In Fig. 3, the d-axis component of reference voltage vector in the rotor frame is generated by using flux neural network controller to tackle the flux error, and the q-axis component of reference voltage vector in the rotor frame is generated by using torque fuzzy controller to tackle the torque error.

The two components of reference voltage vector in the stationary frame are inputted into SVM module and generate PWM signal controlling switch state of the inverter.

**B. Design fuzzy controller of torque**

*Fuzzy Variables and Membership Functions*

The torque fuzzy controller also has two input variables and one output variable. Input variables: torque error  $E_T$  and change rate of torque error  $\Delta E_T$ . Output variable: q-axis component of reference voltage vector  $u_{qr}$ .  $E_T$  has five fuzzy subsets: PL, PS, Z, NS, NL.  $\Delta E_T$  has three fuzzy subsets: P, Z, N.  $u_{qr}$  has five fuzzy subsets: PL, PS, Z, NS, NL (Fig. 4).

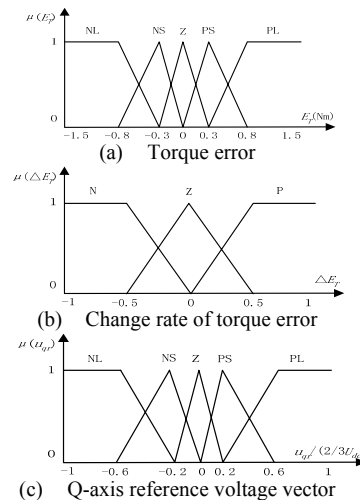


Figure 4. The fuzzy membership functions of torque controller

*Fuzzy Control Rules*

Fuzzy control rules apply IF-THEN form. The rule of torque fuzzy controller  $R_i$  can be written as.  $R_i : \text{If } E_T = A_i \text{ and } \Delta E_T = B_j \text{ then } u_{qr} = C_{ij}$ ; Where:  $A_i$ 、 $B_j$ 、 $C_{ij}$  is some fuzzy subset of  $E_T$ 、 $\Delta E_T$  and  $u_{qr}$  respectively.

The total number of rules of torque fuzzy controller is 15. As Tab. II shows.

TABLE II . MC ACTIVE AND ZERO VECTORS

$u_{qr}$	$E_T$				
	$NL$	$NS$	$Z$	$PS$	$PL$
$\Delta E_T$	$NL$	$NS$	$Z$	$PS$	$PL$
$N$	$PL$	$PL$	$PS$	$Z$	$Z$
$Z$	$PL$	$PS$	$Z$	$NS$	$NL$
$P$	$Z$	$Z$	$NS$	$NL$	$NL$

C. *Design of flux neural network controller*

*The neural network structure of flux*

The flux reference voltage vector  $U_{dr}$  was realized by BP neural network. Its structure show in Fig. 5.

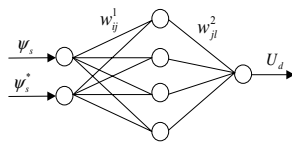


Figure 5. neural-network structure of stator flux

*The neural network learning algorithm of flux*

The neural network can signify arbitrary non-linear function. Three layer BP neural network contain input layer, hide layer and output. The relationship among three layer as follow.

$$v_j^1(n) = \sum \omega_{ij}^1(n) u_i(n) \quad (4)$$

$$v_k^2(n+1) = \sum \omega_{jk}^2(n) v_j^1(n) \quad (5)$$

$$y_k(n+1) = f(v_k^2(n+1)) \quad (6)$$

Where  $k$  is the output layer variable;  $j$  is the hide layer variable;  $v$  is the neural network unit;  $y$  is the neural network output;  $\omega_{ij}(n)$  is the neuron weight from  $i$  to  $j$ ;  $f$  is the activate function. Suppose  $d(n)$  is the expectation output of neural output, then transient error vector can expressed as:

$$e(n) = d(n) - y(n) \quad (7)$$

The target function can defined as:

$$E(n) = \frac{1}{2} e(n)^T e(n) \quad (8)$$

According to the shortest down rules can obtain the amendment quantity  $\omega_{im}(n)$

$$\Delta \omega_{im}(n) = -\eta \frac{\partial E(n)}{\partial \omega_{im}(n)} \quad (9)$$

In order to keep the stability of the algorithm, momentum factor  $\alpha$  is quoted in the weight:

$$\Delta \omega_{im}(n) = -\eta \frac{\partial E(n)}{\partial \omega_{im}(n)} + \alpha \Delta \omega_{im}(n-1) \quad (10)$$

Theoretical analysis verify this network structure can mapping arbitrary nonlinearity function only hide layer quantity is enough. The input parameter is flux given value  $\psi_s^*$  and flux calculated value, the output variable is the reference voltage vector  $U_d$ . Activated function adopt to tansig, hide layer unit is 4, according to learning rate and target error adjust the quantity of hide layer. The training result shown that the target error can received less than 0.01 when hide layer quantity is 4, learning rate is 0.2 and training frequency.

IV. MATRIX CONVERTER SPACE VECTOR

A. *working principle of matrix converter*

A MC is an AC-AC converter, with  $m \times n$  bidirectional switches, which connects an  $m$ -phase voltage source to an  $n$ -phase load. The three-phase,  $3 \times 3$  switches, MC shown in Fig. 6 is the most interesting. It connects a three phase voltage source to a three-phase load[12].

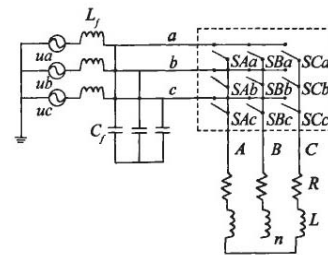


Figure 6. The topology of matrix converter

In the MC shown in Fig. 6,  $v_{si}$ ,  $i = \{A, B, C\}$  are the source voltages,  $i_{si}$ ,  $i = \{A, B, C\}$  are the source currents,  $v_{jn}$ ,  $j = \{a, b, c\}$  are the load voltages,  $i_{jn}$ ,  $j = \{a, b, c\}$  are the load currents,  $v_i$ ,  $i = \{A, B, C\}$  are the MC input voltages and  $i_i$ ,  $i = \{A, B, C\}$  are the input currents. A switch,  $S_{ij}$ ,  $i = \{A, B, C\}$ ,  $j = \{a, b, c\}$  can connect phase  $i$  of the input to phase  $j$  of the load. With a suitable switching strategy, arbitrary voltages  $v_{jN}$  at arbitrary frequency can be synthesized. Switches are characterized by the following equation.

$$S_{ij} = \begin{cases} 0 & \text{with } S_{ij} \text{ is open} \\ 1 & \text{with } S_{ij} \text{ is close} \end{cases} \quad (11)$$

A mathematical model of MC can be derived from Fig. 6 as follows:

$$\begin{bmatrix} v_{aN}(t) \\ v_{bN}(t) \\ v_{cN}(t) \end{bmatrix} = \begin{bmatrix} S_{Aa}(t) & S_{Ba}(t) & S_{Ca}(t) \\ S_{Ab}(t) & S_{Bb}(t) & S_{Cb}(t) \\ S_{Ac}(t) & S_{Bc}(t) & S_{Cc}(t) \end{bmatrix} \cdot \begin{bmatrix} v_A(t) \\ v_B(t) \\ v_C(t) \end{bmatrix} \quad (12)$$

$$\begin{bmatrix} i_A(t) \\ i_B(t) \\ i_C(t) \end{bmatrix} = \begin{bmatrix} S_{Aa}(t) & S_{Ab}(t) & S_{Ac}(t) \\ S_{Ba}(t) & S_{Bb}(t) & S_{Bc}(t) \\ S_{Ca}(t) & S_{Cb}(t) & S_{Cc}(t) \end{bmatrix} \cdot \begin{bmatrix} i_a(t) \\ i_b(t) \\ i_c(t) \end{bmatrix} \quad (13)$$

The conventional three-phase to three-phase matrix converter's modulation process consists of two processes of AC-DC and DC-AC. It is shown in Fig. 7.

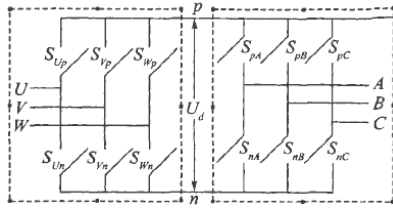


Figure 7. The topology of 3 x 3 matrix converter

The control signal for bidirectional switches come from the control circuit and drive circuits. The ratio cycles of 9 bidirectional switches correspond to a 3 x 3 matrix in each switching period.

**B. DC-AC converter space vector modulation**

6 power switches of inverter with 8 possible combinations shown in Fig. 8 are corresponding to effective voltage space vector  $U_1-U_6$  and 2 zero vector  $U_0, U_7$ . The phase angle between one effective voltage space vector and adjacent one is 60 degrees. They constitute 6 uniform segments. The three digits in brackets express the linking state between three-phase output A,B,C and the input DC, such as M=101 which represents the switching of the switches  $S_{pA}, S_{nB}, S_{pC}$ .

The output voltage space vectors and the corresponding switching states are represented in Fig. 5.

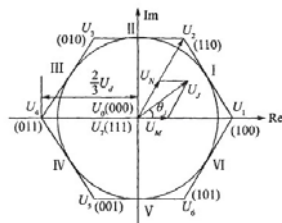


Figure 8. The composition of output voltage vector and switching states

Any expected output voltage space vector  $U_J$  is formed by adjacent two basic output voltage vectors  $U_M, U_N$  and zero output voltage  $U_0$  or  $U_7$ . suppose the angle between  $U_J$  and  $U_M$  is  $\theta_J$ .

$$U_J = d_M U_M + d_N U_N + d_0 U_0 \quad (14)$$

Where  $d_M, d_N$  and  $d_0$  are the ratio cycles of  $U_M, U_N$  and  $U_0$  respectively. And

$$d_M = T_M / T_\delta = m_v \sin(60^\circ - \theta_J) \quad (15)$$

$$d_N = T_N / T_\delta = m_v \sin \theta_J \quad (16)$$

$$d_0 = 1 - d_M - d_N \quad (17)$$

Where  $T_M, T_N$  is the switching time of vectors  $U_M$  and  $U_N$  respectively.  $T_\delta$  is the switching period of PWM.  $m_v$  is the modulation index of output voltage. And

$$m_v = (2/3)^{1/2} U_{om} / (U_{im} m_c \cos \phi) \quad (18)$$

Where  $U_{om}$  and  $U_{im}$  are the amplitude of output and input voltage,  $m_c$  is the input current modulation index, generally set  $m_c = 1$ ,  $\phi$  is the input power factor angle.

When the rotating space vector  $U_J$  locates in a segment, the local average of output voltage can be formed by two adjacent basic voltage space vectors constituting this segment and one zero voltage space vector.

**C. AC-DC converter space vector modulation**

The space vector modulation process of AC-DC is completely similar to the modulation process of DC-AC. Its topology is represented in the left dotted line frame of Fig. 7. The corresponding formulas are similar as well. After rectification, the DC voltage is.

$$U_d = 1.5 m_c U_{im} \cos \phi \quad (19)$$

**D. Matrix converter space vector modulation**

Three-phase matrix converter module includes nine bidirectional switches as shown in Fig. 6. There are 27 possible switching configurations (SCs), only 21 SCs can be used to implement the DTC algorithm for MC as shown in Tab. II: group I ( $\pm 1, \pm 2, \dots, \pm 9$ ) consists of the SCs which have two output phases connected to the same one of the other input phase, group II ( $0_a, 0_b, 0_c$ ) consists of the SCs which have all output phases connected to a common input phase. For each SCs, the corresponding output line-to-neutral voltage vector and input line current vector have the fixed directions as represented in Fig. 9.

TABLE III. MC ACTIVE AND ZERO VECTORS

Group	Vector	A B C	$V_0$	$\alpha_0$	$I_1$	$\beta_1$
I	+1 <sub>ac</sub>	a b b	$2/3 V_{ab}$	0	$2/\sqrt{3} i_a$	$-\pi/6$
	-1 <sub>ac</sub>	b a a	$-2/3 V_{ab}$	0	$-2/\sqrt{3} i_a$	$-\pi/6$
	+2 <sub>ac</sub>	b c c	$2/3 V_{bc}$	0	$2/\sqrt{3} i_b$	$\pi/2$
	-2 <sub>ac</sub>	c b b	$-2/3 V_{bc}$	0	$-2/\sqrt{3} i_b$	$\pi/2$
	+3 <sub>ac</sub>	c a a	$2/3 V_{ca}$	0	$2/\sqrt{3} i_c$	$7\pi/6$
	-3 <sub>ac</sub>	a c c	$-2/3 V_{ca}$	0	$-2/\sqrt{3} i_c$	$7\pi/6$
	+4 <sub>ac</sub>	b a b	$2/3 V_{ab}$	$2\pi/3$	$2/\sqrt{3} i_b$	$-\pi/6$
	-4 <sub>ac</sub>	a b a	$-2/3 V_{ab}$	$2\pi/3$	$-2/\sqrt{3} i_b$	$-\pi/6$
	+5 <sub>ac</sub>	c b c	$2/3 V_{bc}$	$2\pi/3$	$2/\sqrt{3} i_c$	$\pi/2$
	-5 <sub>ac</sub>	b c b	$-2/3 V_{bc}$	$2\pi/3$	$-2/\sqrt{3} i_c$	$\pi/2$
	+6 <sub>ac</sub>	a c a	$2/3 V_{ca}$	$2\pi/3$	$2/\sqrt{3} i_a$	$7\pi/6$
	-6 <sub>ac</sub>	c a c	$-2/3 V_{ca}$	$2\pi/3$	$-2/\sqrt{3} i_a$	$7\pi/6$
	+7 <sub>ac</sub>	b b a	$2/3 V_{ab}$	$4\pi/3$	$2/\sqrt{3} i_c$	$-\pi/6$
	-7 <sub>ac</sub>	a a b	$-2/3 V_{ab}$	$4\pi/3$	$-2/\sqrt{3} i_c$	$-\pi/6$
	+8 <sub>ac</sub>	c c b	$2/3 V_{bc}$	$4\pi/3$	$2/\sqrt{3} i_e$	$\pi/2$
	-8 <sub>ac</sub>	b b c	$-2/3 V_{bc}$	$4\pi/3$	$-2/\sqrt{3} i_e$	$\pi/2$
	+9 <sub>ac</sub>	a a c	$2/3 V_{ca}$	$4\pi/3$	$2/\sqrt{3} i_e$	$7\pi/6$
	-9 <sub>ac</sub>	c c a	$-2/3 V_{ca}$	$4\pi/3$	$-2/\sqrt{3} i_e$	$7\pi/6$
II	0 <sub>a</sub>	a a a	0	-	0	-
	0 <sub>b</sub>	b b b	0	-	0	-
	0 <sub>c</sub>	c c c	0	-	0	-

The other 6 SCs have the output phases connected to the different input phases. In this case, the output voltage vector and input current vector have variable directions and can not be usefully used.

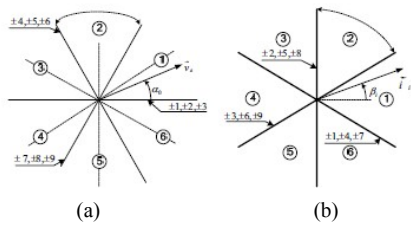


Figure 9. (a)The output line-to-neutral voltage vectors  
(b)The input line current vectors

V. NOVEL DTC-SVM USE MATRIX CONVERTER

The novel DTC-SVM method will apply the direct SVM technique to overcome the disadvantages of the conventional DTC for matrix converter[13],[14]. According to the input voltage line to neutral vector sector location, to combine the desired imaginary non-zero VSI voltage vector, the two non-zero voltage vectors will be selected.

The criteria utilized to implement the switching patterns for the matrix converter can be explained referring to the following example.

We can assume the imaginary VSI voltage vector is V1, and the input voltage line-to-neutral vector [15] is located in sector 1 as shown in Fig. 10 .

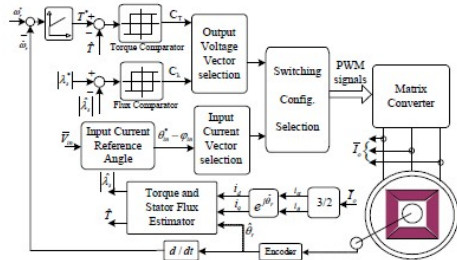


Figure 10. Block diagram of novel DTC-SVM for MC

From Tab. III, in order to generate a voltage vector in the same direction of V1, there are 6 possible SCs ( $\pm 1, \pm 2, \pm 3$ ). According to the input voltage vector location, there are only 3 SCs having the voltage vectors as same direction to V1: +1, -2 and -3. To synthesize the input current vector to be in phase with the input voltage vector located in sector 1, two SCs finally selected are +1 and -3. The switching table based on these criteria is shown in Tab. IV.

As shown in Fig. 9, the output voltage of matrix converter for each SCs is calculated.

$$V_s = \begin{bmatrix} S_{aA} & S_{aB} & S_{aC} \\ S_{bA} & S_{bB} & S_{bC} \\ S_{cA} & S_{cB} & S_{cC} \end{bmatrix} \begin{bmatrix} V_a \\ V_b \\ V_c \end{bmatrix} = T \begin{bmatrix} V_a \\ V_b \\ V_c \end{bmatrix} \quad (20)$$

Where the switching function  $S_{ij}$  is 1 when the switch joining input line  $i$  to output line  $J$  is ON and is 0 otherwise,  $i=a,b,c$  and  $J=A,B,C$ . Matrix  $T$  represents the status of each switching configuration in Tab. II .

The input voltage vector of induction motor in the stationary reference frame for each sampling period.

$$\vec{v}_s = \begin{bmatrix} \vec{v}_{sd} \\ \vec{v}_{sq} \end{bmatrix} = \frac{2}{3} \begin{bmatrix} 1 & -\frac{1}{2} & -\frac{1}{2} \\ 0 & \frac{\sqrt{3}}{2} & \frac{\sqrt{3}}{2} \end{bmatrix} [t_1 T_x + t_2 T_y] \begin{bmatrix} V_a \\ V_b \\ V_c \end{bmatrix} \quad (21)$$

TABLE IV.  
DTC-SVM SWITCHING TABLE USING MC

Sector of $v_s$	1	2	3	4	5	6
Duty ratio	$t_1$	$t_2$	$t_1$	$t_2$	$t_1$	$t_2$
$V_{sd}$	$+V_{sc1}$	$+V_{sc2}$	$+V_{sc3}$	$+V_{sc4}$	$+V_{sc5}$	$+V_{sc6}$
$V_{sq}$	$+V_{sc1}$	$+V_{sc2}$	$+V_{sc3}$	$+V_{sc4}$	$+V_{sc5}$	$+V_{sc6}$
$V_{sd}$	$+V_{sc1}$	$+V_{sc2}$	$+V_{sc3}$	$+V_{sc4}$	$+V_{sc5}$	$+V_{sc6}$
$V_{sq}$	$+V_{sc1}$	$+V_{sc2}$	$+V_{sc3}$	$+V_{sc4}$	$+V_{sc5}$	$+V_{sc6}$
$V_{sd}$	$+V_{sc1}$	$+V_{sc2}$	$+V_{sc3}$	$+V_{sc4}$	$+V_{sc5}$	$+V_{sc6}$
$V_{sq}$	$+V_{sc1}$	$+V_{sc2}$	$+V_{sc3}$	$+V_{sc4}$	$+V_{sc5}$	$+V_{sc6}$

From Fig. 9, the duty ratios of the two non-zero SCs are calculated as follows.

$$t_1 V_x + t_2 V_y = V_{VSI}$$

$$\frac{t_1 V_x}{\sin(\pi/6 - \alpha_i)} = \frac{t_2 V_y}{\sin(\pi/6 + \alpha_i)} \quad (22)$$

$$t_1 + t_2 = 1$$

Finally,

$$t_1 = \frac{\sin(\pi/6 - \alpha_i)}{\cos(\alpha_i)}$$

$$t_2 = \frac{\sin(\pi/6 + \alpha_i)}{\cos(\alpha_i)} \quad (23)$$

The induction motor stator flux can be obtained from the calculated input voltage and the measured stator currents.

$$\vec{\varphi}_s = \int (\vec{v}_s - R_s \vec{i}_s) dt \quad (24)$$

The motor estimated torque can be obtained.

$$\vec{T} = \frac{3n_p}{2} (\vec{\varphi}_{sd} i_{sq} - \vec{\varphi}_{sq} i_{sd}) \quad (25)$$

VI. SIMULATION OF DTC-SVM USING MC

A. The simulation model of DTC-SVM using MC

In order to verify the behavior of the proposed scheme, some simulation has been carried out assuming a sampling period of  $50\mu s$ . The system simulation model is shown in Fig. 11. The machine utilized for simulations is a three-phase 3KW cage induction motor:  $P_n=2.2kw$ ,  $U_n=380V$ ,  $R_s=4.35\Omega$ ,  $R_r=0.43\Omega$ ,  $L_s=2mH$ ,  $L_r=2mH$ ,  $L_m=69.31mH$ ,  $J=0.089 kg \cdot m^2$ ,  $P=2$ .

The whole system has been simulated using the Simulink package. Equation (12) and Equation (13) are used to obtain the matrix output voltages and the input currents respectively, thus assuming ideal switching devices. The mains filtered line current is calculated on the basis of the matrix input current.

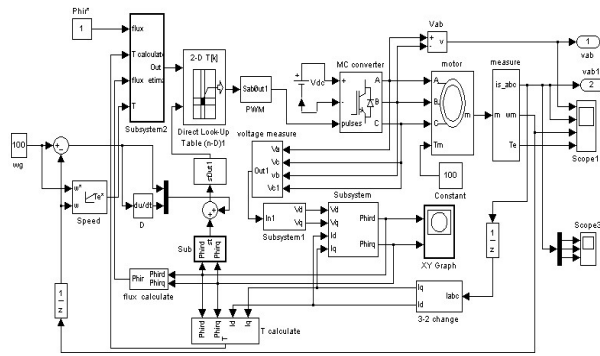


Figure 11. The simulation model MC-DTC for MC

**B. The simulation result of DTC-SVM using MC**

Both steady states at the high and low speed, the dynamic performance are shown to verify the effectiveness of the proposed MC-DTC method.

At the high speed operation, induction motor is running at speed 1000 rpm, rated load torque 25 Nm and flux reference 0.6 Wb. The simulation result show in Fig. 12-Fig. 14.

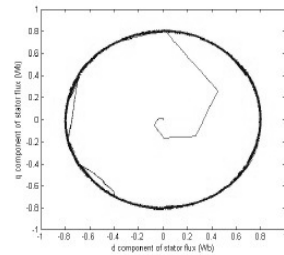


Figure 12. The simulation of flux at 1000rpm, 25Nm for MC-DTC

In relation with the DTC-SVM for MC scheme, Fig. 12 shows a good performance in terms of stator flux. As it can be seen in Fig. 12, stator flux shows a circle waveform.

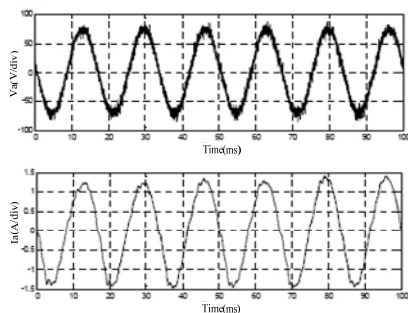


Figure 13. Input voltage and current of phase-a for MC-DTC

Fig. 13 shows the input voltages and current in phase-a during the steady state operation. It can be seen that the currents are sinusoidal and in phase with the voltages meaning that the power factor is unity.

Fig. 14 shows stator flux and electromagnetic torque of the induction motor fully following the reference values. Furthermore, the stator currents have sinusoidal waveforms. This figure emphasizes the good performance of the drive system with regard to the implementation of the novel MC-DTC method.



Figure 14. The simulation of current and torque at 1000rpm for MC-DTC

At the low speed operation, induction motor is running at a very low speed 100 rpm, load torque 20 Nm and flux reference 0.6Wb. The simulation result show in Fig. 15-Fig. 16.

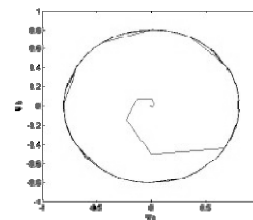


Figure 15. The simulation of flux at 100rpm, 25Nm for MC-DTC

Fig. 15 shows the flux magnitude perfectly follows the flux reference and stator current still has a sinusoidal waveform.

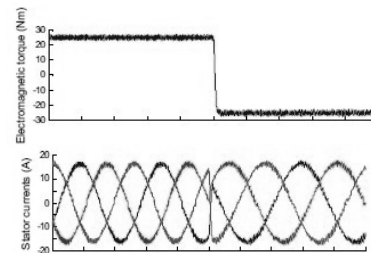


Figure 16. Simulation during a load torque step command from +25Nm to -25Nm the torque and current at 100rpm for MC-DTC

Fig. 16 shows the dynamic performances of the novel control method at the rotor speed 100rpm and load torque change as a step command from +25 Nm to -25 Nm. The electromagnetic torque shows a very good response and the stator current waveforms are almost sinusoidal immediately right after the step command.

**VII. EXPERIMENT OF DTC-SVM FOR MC**

**A. The system setup of MC-DTC**

The novel method had been tested. The parameters are same as simulation parameters. The motor was fed by a 7.5 KW Motor. The MC-DTC algorithms were implemented in TMS320LF2407 DSP achieving a sample period of 50µs. The four-step commutation process, required when bidirectional switches are used, was implemented in a FPGA. A current-controlled hysteresis brake provides the load torque. A block diagram of the system setup is shown in Fig. 17.

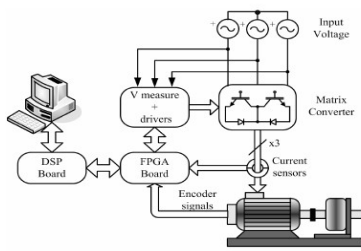


Figure 17. The system setup of DTC-SVM using MC

**B. The experiment result of DTC-SVM using MC**

At the high speed operation, induction motor is running at speed 1000 rpm, rated load torque 0.2Nm and flux reference 0.6 Wb. The experiment result show in Fig. 18-Fig. 19.

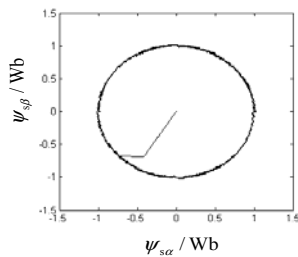


Figure 18. The experiment result of flux at 1000rpm, 25Nm for MC-DTC

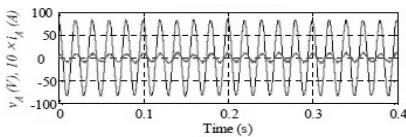


Figure 19. Input voltage, current and spectrum corresponding of phase-a for MC-DTC at 1000rpm

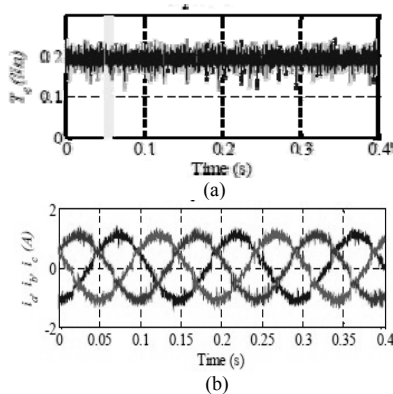


Figure 20. During a load torque step command from +25Nm to -25Nm the torque, current and flux at 100rpm for MC-DTC

It can be seen from Fig. 18-Fig. 20, stator current, electromagnetic torque, stator voltage and stator flux performance at high speed respectively. As regard the ripple, the proposed novel method clearly improves the performance of both the torque and flux. Furthermore, in the case of torque, the type of the applied vectors is also shown. At the same time, the inner torque hysteresis bands in the proposed method are identical to the torque hysteresis bands in the classical method. Thus, the outer bands in the proposed method can be seen as security

limits above which the large vectors are used in order to quickly force the torque towards its reference value.

The output currents  $i_a$ ,  $i_b$ ,  $i_c$ , for the classical and the proposed method are depicted in Fig. 20(a) and Fig. 20(b) respectively. As expected, there is a significant decrease in the current ripple. This fact alleviates the switches stress, hence reducing the switching losses.

Fig. 19 shows that the input current  $i_A$  and the corresponding line-to-neutral input voltage  $v_A$  for the proposed method. In case the input line current  $i_A$  is in phase with the line-to-neutral voltage  $v_A$ . This confirms the effectiveness of methods regarding the PF correction capability.

At the low speed operation, induction motor is running at a very low speed 100 rpm, load torque 25Nm and flux reference 0.6Wb. The experiment result show in Fig. 21-Fig. 23.

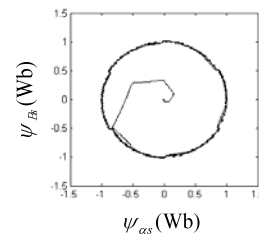


Figure 21. The experiment result of flux at 100rpm, 25Nm for MC-DTC

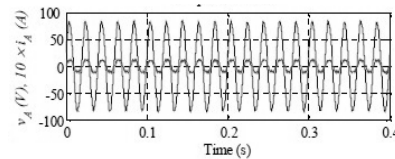


Figure 22. Input voltage, current and spectrum corresponding of phase-a for MC-DTC

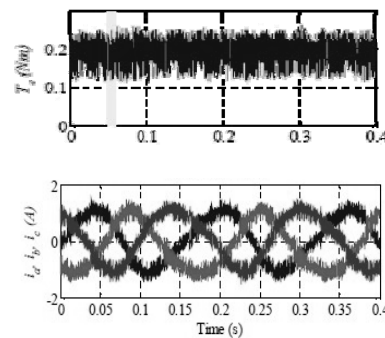


Figure 23. During a load torque step command from +25Nm to -25Nm the torque, current and flux at 100rpm for MC-DTC

Fig. 21-Fig. 23 show that the stator flux and input line current with higher amplitude in the low frequency range when compared with the high speed. However, this is not seen as a constraint since a re-design of the MC input filter would be enough to overcome this drawback.

In order to study the dependency of the torque ripple with respect to both the torque reference and the motor speed, several tests were carried out at low-speed. The standard deviation of the torque was calculated to measure the torque ripple.

The results showed better performance of the proposed novel method over all the motor operating speed.

#### VIII. CONCLUSION

This paper presents a new MC-DTC method for induction motor based on fuzzy-neural network space vector modulation. The advantages of the DTC method have been successfully combined with the SVM method on matrix converter. A new switching table for the DTC-SVM which fully controls the induction motor requirements is suggested, besides perfectly controlling the input unity power factor. The simulation and experiment results on the induction motor at the low and high speed range are shown to validate the effectiveness of the new control scheme. Furthermore, the novel control strategy shows the better input current harmonic spectrum and low-speed performance as compared to the conventional MC-DTC method and it can make the flux and torque small and stable. It has advantages and good future, it is worth further studying.

#### ACKNOWLEDGMENT

The authors would like to thank the Scientific Research Fund of Hunan Provincial education department and the reviewers for their valuable comments and suggestions.

#### REFERENCES

- [1] D. Casadei, F. Profumo, and A. Tani, FOC and DTC: two viable schemes for induction motors torque control, *IEEE Trans. Power Electron*, vol. 17, No. 5, pp. 779-787, 2007.
- [2] G. S. Buja and M. P. Kazmierkowski, Direct torque control of PWM Inverter-Fed AC Motors-A survey, *IEEE Trans. on Industrial Electronics*, vol. 51, No. 4, pp. 744-758, August 2008.
- [3] Xin Wei, Dayue Chen, and Chunyu Zhao, A New direct torque control strategy of induction motors based on duty ratio control technique, *Proceedings of the Chinese Society for Electrical Engineering*, vol. 25, No. 5, pp. 93-97, 2008.
- [4] S. Mir and M. E. Elbuluk, Precision torque control in Inverter-Fed induction machines using fuzzy logic, *Proceedings of the 26th IEEE Power Electronics Specialists Conference(PESC)*, vol. 1, pp. 396-401, 1995.
- [5] Xiyang Ding, Qiang Liu, Xiaona Ma, Xiaoran He, and Qing Hu, The fuzzy torque control of induction motor based on space vector modulation, *Third International Conference on Natural Computation*, 2009.
- [6] S. Mir and M. E. Elbuluk, Precision torque control in Inverter-Fed induction machines using fuzzy logic, *Proceedings of the 26th IEEE Power Electronics Specialists Conference(PESC)*, vol. 1, pp. 396-401, 2005.
- [7] Xiyang Ding, Qiang Liu, Xiaona Ma, Xiaoran He, and Qing Hu, The fuzzy torque control of induction motor based on space vector modulation, *Third International Conference on Natural Computation*, 2009.
- [8] Zhijun Jiang, Shimiao Hu, and Wenhui Cao, A new fuzzy logic torque control scheme based on vector control and direct torque control for induction machine, *The 3rd International Conference on Innovative Computing Information*, 2010.
- [9] LEE K B, BLAABJERG F, improved direct torque control for sensorless matrix converter drives with constant switching frequency and torque ripple reduction, *international journal of control, automation and system*, 2009,4(1):113-123.
- [10] C. Lascu, I. Boldea, and F. Blaabjerg, Very-low-speed variable-structure control of sensorless induction machine drives without signal injection, *IEEE Trans. Ind. Appl.*, vol. 41, no. 2, pp.591-598, Mar./Apr. 2008.
- [11] C. Lascu, I. Boldea, and F. Blaabjerg, Direct torque control of sensorless induction motor drives: a sliding-mode approach, *IEEE Trans. Ind. Appl.*, vol. 40, no.2, pp.582-590, Mar/Apr. 2008
- [12] Z. Xu and M. F. Rahman, Direct torque and flux regulation of an IPM synchronous motor drive using variable structure control approach, *IEEE Trans. Power Electron.*, vol.22, no. 6, pp.2487-2498, Nov. 2010.
- [13] V. I. Utkin, Sliding mode control design principles and applications to electric drives, *IEEE Trans. Ind.Electron.*, vol.40, no. 1, pp.23-36, Feb. 2003.
- [14] C. Lascu and A. M. Traynadlowski, Combining the principles of sliding mode, direct torque control, and space vector modulation in a high-performance sensorless AC drive, *IEEE Trans. Ind. Appl.*, vol.40, no. 1, pp. 170-177, Jan./Feb. 2007.
- [15] A. Naassani, E. Monmasson, and J. P. Louis, Synthesis of direct torque and rotor flux control algorithms by means of sliding-mode theory, *IEEE Trans. Ind.Electron.*, vol.52, no.3, pp. 785-799, June. 2010.

**Cai Bin-jun** was born in xiangtan, Hunan, on march 11, 1976. He received the B.S. and M.S. degrees in electrical and electronic engineering from Xiangtan University, Hunan, China, in 1997 and 2007, respectively.

From 2004 to 2007, he was with the Institute of Information Technology, Xiangtan University, Xiangtan, China. In 2007, he joined the School of Hunan Institute of Engineering. His research interests include electric machine drives, power electronics, and wind power generations.